ChemComm

COMMUNICATION

View Article Online
View Journal | View Issue

Cite this: *Chem. Commun.*, 2023, 59, 635

Received 29th September 2022,
Accepted 11th December 2022

DOI: 10.1039/d2cc05334a

rsc.li/chemcomm

Triphenylamine–anthraquinone based donor–acceptor conjugated microporous polymers for photocatalytic hydroxylation of phenylboronic acids†

Soumitra Sau and Suman Kalyan Samanta *

Triphenylamine-based donor–acceptor conjugated microporous polymers, namely PTPA-AQ and PTPA-AM, were synthesized for the first time *via* Suzuki–Miyaura coupling of tris(4-(4,4,5,5-tetramethyl-1,3,2-dioxaborolan-2-yl)phenyl)-amine as a donor with 2,6-dibromoanthracene-9,10-dione and 2,2′-(2,6-dibromoanthracene-9,10-diylidene)dimalononitrile acceptors for efficient visible-light driven oxidative hydroxylation of various phenylboronic acids. The dimalononitrile derivative having greater acceptor ability showed tunable photophysical properties of PTPA-AM (lower band gap of 1.47 eV and better exciton separation efficiency) as well as porosity (lower Brunauer–Emmett–Teller (BET) surface area of 43 m^2 g^{-1}). PTPA-AQ having higher BET surface area (400 m^2 g^{-1}), suitable HOMO–LUMO positions and an optimal band gap (1.94 eV) showed better photocatalytic activity for the hydroxylation with yields up to 96%.

Photocatalysts can accelerate chemical reactions by using light, thus avoiding the use of toxic substances, strong oxidants or harmful reductants, which satisfies 'society's needs at present in terms of energy and the environment. Over the past few decades, many novel photocatalytic materials including transition-metal complexes,[1–3] and molecular organic dyes[4,5] have been explored for a variety of light-induced chemical transformations because of their strong light absorption ability and efficient separation of excitons. However, these homogeneous photocatalysts suffer from several inherent issues such as catalyst separation after the reaction, use of costly and hazardous metals, and poor stability, which restricts their practical applications. Therefore, the development of heterogeneous and metal-free photocatalysts for photo-induced chemical reactions is of paramount importance. Graphitic carbon nitride (g-C_3N_4) has been explored widely towards such applications because of its excellent visible light absorption capability.[6,7] Of late, porous organic polymers (POPs)[8] including covalent organic frameworks (COFs),[9] hypercrosslinked polymers (HCPs),[10,11] and conjugated microporous polymers (CMPs)[12–14] have attracted much attention for photocatalytic reactions.

Due to the presence of an extended π-conjugated polymer backbone and their diverse synthetic strategies, CMPs represent a unique class of materials.[15] Moreover, the donor–acceptor based CMPs (D–A CMPs) have an alternate array of donor and acceptor moieties throughout the network, which leads to an efficient intramolecular charge transfer (ICT), effective exciton separation, and high charge carrier (electron and hole) mobility resulting in improved photocatalytic activity.[16] The electron rich nature of triphenylamine (TPA) enabled it to be used as a donor moiety for synthesizing D–A CMPs. On the other hand, having a high theoretical specific capacity of 259 mA h g^{-1} and redox activity, anthraquinone containing D–A CMPs have been explored in lithium ion batteries.[17,18] So far, TPA and anthraquinone-containing D–A CMPs have been used in photocatalytic hydrogen evolution from water,[19] in the electro-chemical oxygen reduction reaction (ORR),[20] as a cathode material in lithium ion batteries,[21,22] in supercapacitors,[23] as well as in photocatalytic CO_2 reduction.[24]

Herein, we have synthesized two novel TPA-based D–A CMPs, namely PTPA-AQ and PTPA-AM (Scheme 1) *via* Suzuki–Miyaura cross-coupling reaction between tris(4-(4,4,5,5-tetramethyl-1,3,2-dioxaborolan-2-yl)phenyl)amine (Monomer **1**) as a donor moiety with 2,6-dibromoanthracene-9,10-dione (Monomer **2**) and a modified 2,2′-(2,6-dibromoanthracene-9,10-diylidene)dimalononitrile (Monomer **3**) as acceptors (*cf.* Experimental section, Schemes S2 and S3, ESI†). Suitable modification of the anthraquinone moiety by a Knoevenagel-type condensation with malononitrile produced a stronger acceptor, Monomer **3**, which showed tuning of its photophysical properties such as absorption maximum, band gap, HOMO–LUMO positions and porosity. Both the polymers were tested for the photocatalytic oxidative hydroxylation of phenylboronic acid to phenol for the first time. Among them, PTPA-AQ showed

Department of Chemistry, Indian Institute of Technology Kharagpur, Kharagpur, 721302, India. E-mail: sksamanta@chem.iitkgp.ac.in

† Electronic supplementary information (ESI) available: Experimental and synthetic procedures, characterization, results and supporting figures. See DOI: https://doi.org/10.1039/d2cc05334a

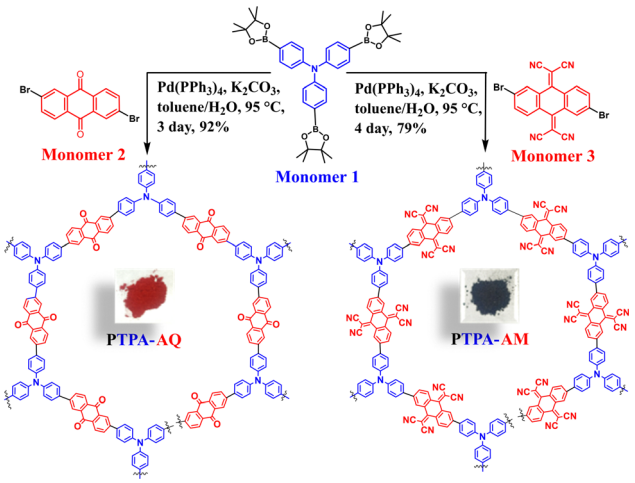

Scheme 1 The synthetic procedures of PTPA-AQ and PTPA-AM.

better photocatalytic activity with a yield up to 96% in correlation with its higher BET surface area (400 $m^2 g^{-1}$), appropriate HOMO–LUMO positions and optimal band gap (1.94 eV).

To investigate the structures of PTPA-AQ and PTPA-AM, the Fourier transform infrared (FTIR) spectra were recorded (Fig. 1a and Fig. S1a, ESI†). The FTIR spectra revealed that the alkyl C–H stretching vibration of the boronic ester group in the TPA moiety at 2982 cm^{-1} was abolished completely in both the polymers, which indicated successful polymerization. On the other hand, the characteristic C=O stretching frequency of anthraquinone at 1680 cm^{-1} was retained in PTPA-AQ and the –CN stretching frequency at 2218 cm^{-1} also remained in PTPA-AM, indicating that the corresponding monomer units were incorporated into the respective polymers. In addition, the peaks at 1575 cm^{-1} are due to the stretching vibrations of the aromatic C=C bonds for PTPA-AQ and PTPA-AM. Solid-state ^{13}C CPMAS NMR spectra of both the CMPs showed that the characteristic aromatic carbon connected to the nitrogen of triphenylamine appeared at ~145 ppm (Fig. 1b and Fig. S1b, ESI†). The corresponding peak for the carbonyl carbon of the anthraquinone unit in PTPA-AQ appeared at ~183 ppm while all other aromatic carbons in both the CMPs were located at ~115–140 ppm. Therefore, the results of FT-IR and the solid-state ^{13}C NMR spectra confirmed the successful construction of both PTPA-AQ and PTPA-AM. X-ray photoelectron spectroscopy (XPS) showed characteristic peaks at ~283, ~398 and ~530 eV for C 1s, N 1s and O 1s, respectively, depicting the surface elemental composition of PTPA-AQ (Fig. S2, ESI†). Thermogravimetric analysis (TGA) of the CMPs revealed that PTPA-AQ and PTPA-AM were stable up to 374 °C and 340 °C, respectively, with 5% weight loss (Fig. S3, ESI†). Up to 80% weight was retained for both the CMPs at an elevated temperature of 570 °C ensuring their high thermal endurance. Scanning electron microscopy (SEM) images revealed that PTPA-AQ has a small island-like morphology with many holes, while PTPA-AM has a similar morphology with agglomerated particles (Fig. 2c and Fig. S4a, ESI†). The presence of C, N and O in PTPA-AQ, and C and N in PTPA-AM was confirmed from the corresponding EDAX profile (Fig S5, ESI†). The results obtained from the TEM images also showed the perforated structures similar to the SEM images (Fig. 1d and Fig. S4b, ESI†). The powder X-ray diffraction (PXRD) profiles supported the amorphous nature (broad peak at ~22°) of both the CMPs without any sharp diffraction peaks (Fig. S6, ESI†).

To gain further information about their porosity, the N_2 adsorption–desorption isotherm was recorded at 77 K (Fig. 2 and Fig. S7, ESI†). The Brunauer–Emmett–Teller (BET) surface areas of PTPA-AQ and PTPA-AM were calculated to be 400 $m^2 g^{-1}$ and 43 $m^2 g^{-1}$, respectively. The significant decrease in BET surface area for PTPA-AM is possibly due to the presence of two malononitrile units within the acceptor moiety that could block the pores effectively. The pore size distribution of PTPA-AQ displayed the coexistence of micropores (mainly centered at 1.9 nm) as well as mesopores (centered at 4 nm) indicating the presence of hierarchical porosity. In addition, the total pore volume and pore diameter of PTPA-AQ were calculated as 0.18 $cm^3 g^{-1}$ and 4.8 nm, respectively.

The influence of the acceptor moieties was investigated using the UV-Vis-NIR diffuse reflectance spectra, which showed a broad absorption from 400–750 nm with a maximum at 482 nm for PTPA-AQ (Fig. 3a). However, a wider absorption

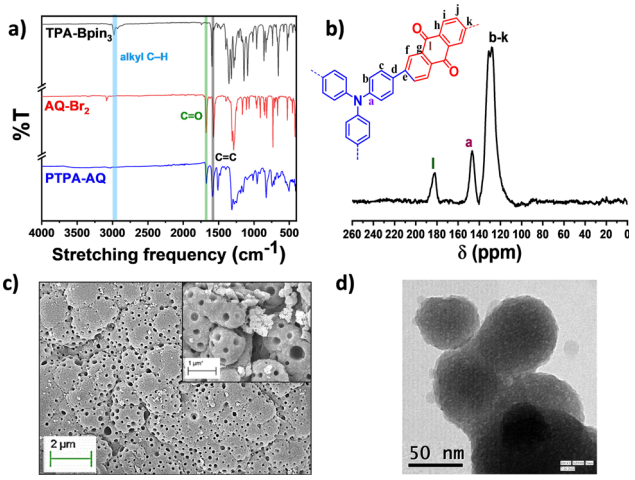

Fig. 1 (a) FT-IR spectra of PTPA-AQ in comparison with Monomer **1** and Monomer **2**. (b) Solid state ^{13}C CPMAS NMR spectrum, (c) SEM image and (d) TEM image of PTPA-AQ.

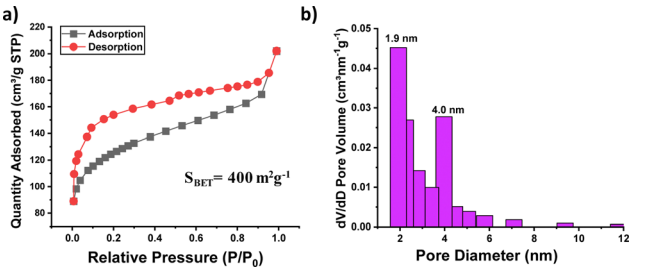

Fig. 2 (a) Nitrogen adsorption–desorption isotherm at 77 K and (b) pore size distribution of PTPA-AQ.

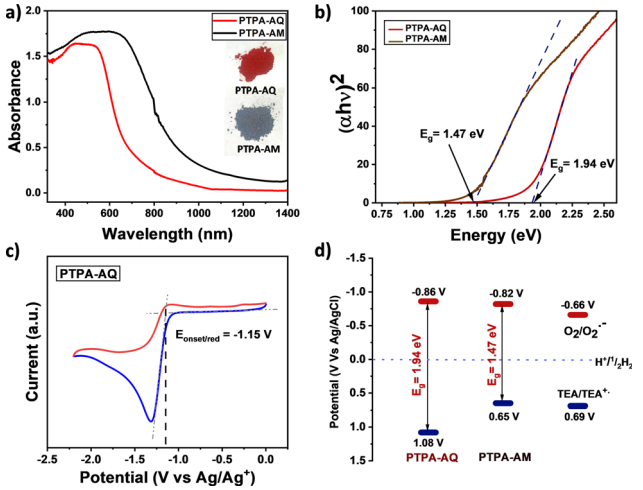

Fig. 3 (a) UV-Vis-NIR diffuse reflectance spectra and (b) the Tauc plot for both the D–A CMPs. (c) CV diagram of PTPA-AQ. (d) HOMO–LUMO positions of the D–A CMPs.

and a red-shifted maximum at 580 nm were observed for PTPA-AM due to an enhanced acceptor ability. Notably, both the CMPs showed absorption covering the entire visible region with a near-infrared (NIR) trail. The optical band gap (E_g), calculated from the Tauc plot (Fig. 3b), showed that PTPA-AM containing a stronger acceptor unit has a narrower band gap (E_g = 1.47 eV) as compared to PTPA-AQ (E_g = 1.94 eV). The energy positions of the lowest unoccupied molecular orbital (LUMO) of the synthesized CMPs were obtained from cyclic voltammetry (CV) measurement (Fig. 3c and Fig. S8, ESI†). The CV profile revealed that due to the presence of a strong acceptor moiety, PTPA-AM has a lower lying LUMO (−0.82 V) than that of PTPA-AQ (−0.86 V). Meanwhile, the reduction potential of $O_2/O_2^{\bullet-}$ at −0.66 V *vs.* Ag/AgCl[25] indicates that both the polymers can sufficiently reduce O_2 to its reactive oxygen species (Fig. 3d). The corresponding energy positions of the highest occupied molecular orbital (HOMO) were 1.08 V and 0.65 V for PTPA-AQ and PTPA-AM, respectively, obtained from the optical band gap values. Density functional theory (DFT) revealed that the HOMO is localized on TPA while the LUMO is on the anthraquinone moiety, confirming their donor–acceptor nature and the theoretical bandgap (2.16 eV) resembles the optical bandgap (Fig. S9, ESI†).

The strong visible light absorption and porous nature of these D–A CMPs enabled them to be used as heterogeneous photocatalysts for visible light-driven oxidative hydroxylation of phenylboronic acid to phenol. By using phenylboronic acid as a model substrate, under the optimal reaction conditions (CH_3CN as solvent, Et_3N as a sacrificial electron donor and reaction time 14 h), PTPA-AQ showed an excellent photocatalytic activity by affording the product in 94% yield (Table S1, ESI†). However, the product yield dropped drastically to 56% for PTPA-AM under similar conditions, possibly due to its low BET surface area, upper lying HOMO and inappropriate band gap (Fig. S10 and S11, ESI†).

Table 1 Visible light-induced oxidative hydroxylation of various substituted phenylboronic acids

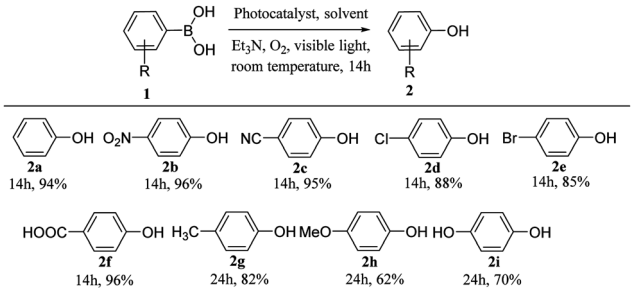

Reaction conditions: phenylboronic acid (0.25 mmol), PTPA-AQ (5 mg), Et_3N (0.375 mmol), CH_3CN (2 mL), white LED (18 W), O_2, room temperature. The yields were calculated after isolation of the product.

The substrate scope of PTPA-AQ-mediated oxidative hydroxylation of phenylboronic acids has been investigated (Table 1). It was observed that the phenylboronic acids containing electron-withdrawing groups (–NO_2, –CN, –Cl, –Br and –COOH) showed higher product yield (**2b–2f**) with respect to that of electron-donating groups (–Me, –OMe and –OH) (**2g–2i**). These results indicated that with increasing the electron-deficiency on the substrate, the electron affinity increases and consequently it can easily react with superoxide anion radicals to form a radical anion intermediate (**A**, Fig. 4). In contrast, an electron donating group makes it difficult to react with superoxide anion radicals leading to a decrease in reactivity.

To elucidate the mechanistic pathway for these photocatalytic reactions, control experiments were performed under different conditions, such as in the absence of light, photocatalyst, triethylamine and oxygen (Table S2, ESI†). In the absence of light and photocatalyst, no conversion was detected

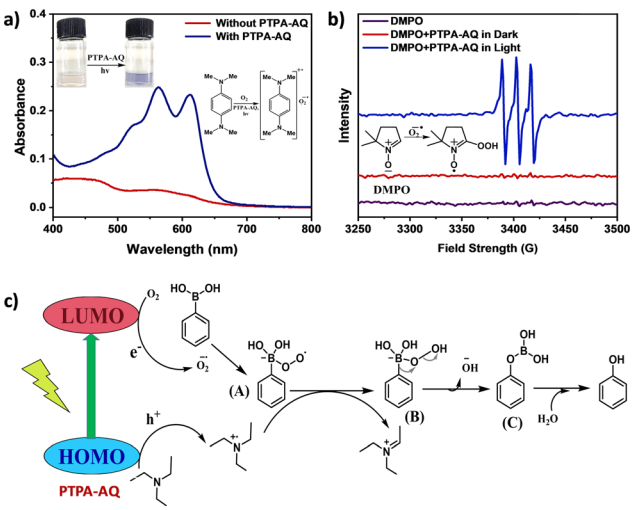

Fig. 4 (a) Absorption spectra of NTPD in acetonitrile in the presence and absence of PTPA-AQ; inset: colorless solution of NTPD turned bluish upon addition of PTPA-AQ under visible light irradiation. (b) EPR signals of DMPO in the absence (black) and presence (red and blue) of PTPA-AQ under dark and light irradiation, respectively. (c) Plausible reaction mechanism for oxidative hydroxylation of phenylboronic acid.

indicating their essential roles in the catalytic transformation. However, a trace amount of phenol was detected when the reaction was performed in the absence of oxygen or trimethylamine, which indicated that adsorbed oxygen might facilitate the reaction.

In addition, similar control experiments were performed employing various reactive oxygen species scavengers like *p*-benzoquinone (*p*-BQ, scavenger for $O_2^{\bullet -}$), NaN_3 (scavenger for singlet oxygen), KI (photo-generated hole scavenger) and $CuCl_2$ (electron scavenger) (Table S3, ESI†).[26] In the presence of *p*-BQ, the yield decreased to 48%, indicating that the superoxide radical anion played a vital role in the reaction mechanism. Upon addition of KI and $CuCl_2$, the yield of phenol decreased significantly to 64% and 43%, respectively, suggesting that the photogenerated holes and electrons also participated in the reaction. However, no significant change in the yield (93%) was observed on addition of NaN_3, indicating that singlet oxygen does not participate in this reaction.

The existence of superoxide as the reactive oxygen species was further established by UV-Vis absorption and electron paramagnetic resonance (EPR) studies (Fig. 4 and Fig. S12, ESI†). The generation of superoxide anion radicals by both PTPA-AQ and PTPA-AM was monitored using *N*,*N*,*N*′,*N*′-tetramethyl-*p*-phenylenediamine (NTPD) in the UV-Vis spectra. Upon photo-excitation in the presence of the photocatalysts, the colorless solution of NTPD turned violet and a corresponding broad band at 450–670 nm was observed indicating the formation of radical cations of NTPD and superoxide radical anions.[26] In the case of PTPA-AM, the intensity of the broad band was lower than that of PTPA-AQ, confirming the greater ability of PTPA-AQ to generate superoxide anion radicals from oxygen. EPR spectra were recorded to further probe the generation of superoxide anion radicals using the spin-trapping agent 5,5-dimethyl-1-pyrroline-*N*-oxide (DMPO). The EPR signals of the sample having DMPO and PTPA-AQ in acetonitrile after 45 min of light illumination referred to the oxidized form of DMPO (Fig. 4b and Fig. S12b, ESI†).[26] Therefore, under visible light irradiation, superoxide anion radicals were generated by the photocatalyst, which participated in the oxidation of DMPO. The EPR signal intensity indicated that PTPA-AQ has a greater ability to form superoxide anion radicals than PTPA-AM. The above results demonstrated that superoxide anion radicals have been generated during the course of the reaction and participated in the reaction mechanism.

A plausible mechanism has been proposed in Fig. 4c. Upon exposure of the photocatalyst to light, photogenerated holes and electrons are separated into their corresponding HOMO and LUMO. The electrons participate in photoreduction of oxygen into a superoxide radical anion and the holes react with triethylamine to produce a radical cation intermediate. The superoxide radical anion then reacts with phenylboronic acid to produce a radical anion intermediate (**A**) which abstracts a proton from the radical cation intermediate of trimethylamine to form intermediate (**B**). After successive rearrangement and hydrolysis, the desired product phenol was formed.

The reusability of PTPA-AQ was evaluated by recycling the photocatalyst up to five-times, which showed no significant drop in the yield (90%) indicating its excellent recycling ability. Moreover, there are no obvious changes in the SEM image or FT-IR spectra of the recovered catalyst compared to the fresh catalyst confirming that the chemical structure and the morphology of the recovered catalyst remained intact even after the 5th cycle (Fig. S13, ESI†). These results support its high stability and reusability towards oxidative hydroxylation of phenylboronic acid.

In summary, two novel TPA-based D–A CMPs, namely PTPA-AQ and PTPA-AM, were successfully synthesized by Suzuki–Miyaura coupling reaction. By changing the acceptor unit, their band gaps, HOMO–LUMO positions and BET surface area were tuned. With increased acceptor ability, the band gap of PTPA-AM decreased to 1.47 eV, and together with its low BET surface area (43 $m^2\ g^{-1}$), it showed a poor photocatalytic activity. PTPA-AQ having higher BET surface area (400 $m^2\ g^{-1}$), optimal band gap (1.94 eV) and suitable band positions showed better performance towards the formation of phenol with yields up to 96%.

S. S. acknowledges IIT Kharagpur for the fellowship. S. K. S. is grateful to SERB, DST (SRG/2019/000922) for funding.

Conflicts of interest

There are no conflicts to declare.

References

1 J. M. R. Narayanam and C. R. J. Stephenson, *Chem. Soc. Rev.*, 2011, **40**, 102–113.
2 L. Shi and W. Xia, *Chem. Soc. Rev.*, 2012, **41**, 7687–7697.
3 D. M. Arias-Rotondo and J. K. McCusker, *Chem. Soc. Rev.*, 2016, **45**, 5803–5820.
4 D. Ravelli, *et al.*, *Chem. Soc. Rev.*, 2013, **42**, 97–113.
5 T.-Y. Shang, *et al.*, *Chem. Commun.*, 2019, **55**, 5408–5419.
6 X. Wang, *et al.*, *Nat. Mater.*, 2009, **8**, 76–80.
7 S. Cao, *et al.*, *Adv. Mater.*, 2015, **27**, 2150–2176.
8 S. Dutta, *et al.*, *Chem. Commun.*, 2022, **58**, 9405–9408.
9 H. Wang, *et al.*, *Chem. Soc. Rev.*, 2020, **49**, 4135–4165.
10 R. Li, *et al.*, *ACS Catal.*, 2016, **6**, 1113–1121.
11 Y. Zhi, *et al.*, *J. Mater. Chem. A*, 2017, **5**, 8697–8704.
12 J.-S. M. Lee and A. I. Cooper, *Chem. Rev.*, 2020, **120**, 2171–2214.
13 S. K. Samanta, *et al.*, *Chem. Commun.*, 2015, **51**, 9046–9049.
14 Z. Qian and K. A. I. Zhang, *Solar RRL*, 2021, **5**, 2000489.
15 Y. Xu, *et al.*, *Chem. Soc. Rev.*, 2013, **42**, 8012–8031.
16 J. W. Jung, *et al.*, *Adv. Mater.*, 2015, **27**, 7462–7468.
17 L. Zhong, *et al.*, *Angew. Chem., Int. Ed.*, 2021, **60**, 10164–10171.
18 M. G. Mohamed, *et al.*, *ACS Appl. Energy Mater.*, 2021, **4**, 14628–14639.
19 W.-J. Xiao, *et al.*, *Macromolecules*, 2020, **53**, 2454–2463.
20 S. Roy, *et al.*, *J. Mater. Chem. A*, 2018, **6**, 5587–5591.
21 W. Huang, *et al.*, *Electrochim. Acta*, 2018, **283**, 1284–1290.
22 C. Su, *et al.*, *ChemElectroChem*, 2020, **7**, 4101–4107.
23 M. G. Kotp, *et al.*, *J. Taiwan Inst. Chem. Eng.*, 2022, **134**, 104310.
24 Y. Wang, *et al.*, *ACS Sustainable Chem. Eng.*, 2022, **10**, 9460–9468.
25 W. Huang, *et al.*, *ACS Catal.*, 2017, **7**, 5438–5442.
26 C. Song, *et al.*, *Appl. Catal., B*, 2021, **287**, 119984.

